

Weak gravitational lensing of intrinsically aligned galaxies

Aram Giahi-Saravani^{*} and Björn Malte Schäfer

Zentrum für Astronomie der Universität Heidelberg, Philosophenweg 12, 69120 Heidelberg, Germany

10 November 2021

ABSTRACT

Subject of this paper is the weak lensing effect on galaxies that show intrinsically correlated ellipticities. In our model, we investigate the distortion of the ellipticity field if the galaxies experience an apparent shift in their position by weak lensing deflection and compare this effect to the shearing effect induced by tidal fields. Starting with a derivation of intrinsic ellipticity spectra by employing a tidal torquing model generating galactic angular momenta, we model the galaxy ellipticity by assuming that the galactic disk forms perpendicularly to the host halo angular momentum direction and derive intrinsic ellipticity E -mode and B -mode spectra from the angular momentum statistics. The lensing effect on the ellipticity field is modeled by employing the methodology developed in the framework of lensing of the cosmic microwave background polarisation. For EUCLID, ellipticity correlations are altered by lensing deflection on multipoles $\ell \gtrsim 1000$ by $\sim 5\%$ for the ellipticity E -modes and by $\sim 30\%$ for the B -modes, while a shallower survey would exhibit larger changes on larger angular scales. In addition to the convolving effect of lensing on the ellipticity spectra we investigate the E/B -mode conversion, and discuss the possibility of measuring correlations between different multipoles which is evoked by the homogeneity breaking effect of the lensing displacement. Our conclusion is that although shape correlations generated by weak gravitational shear is dominant, the shifting effect due to lensing is shaping the ellipticity spectra on small angular scales and causes a number of interesting phenomena, which might be observable by future surveys.

Key words: cosmology: large-scale structure, gravitational lensing, methods: analytical

1 INTRODUCTION

Weak gravitational lensing by the cosmic-large scale structure provides a measurement of the cosmic tidal field and provides sensitivity on cosmological parameters due its dependence on the geometry of the cosmological model and the growth rate of matter perturbations (for reviews, see [Bartelmann & Schneider 2001](#); [Hoekstra & Jain 2008](#); [Bartelmann 2010](#)). Weak lensing data taken by future surveys such as EUCLID, DES and LSST has the potential of putting tight constraints on cosmological parameters and to distinguish between dark energy models and those with modified gravity (for a comprehensive summary, see [Weinberg et al. 2012](#)).

In analysing weak lensing data it is usually assumed that weak lensing is the only effect causing correlations in the shapes of galaxies, which is sadly not the case as correlations in the shapes of neighbouring galaxies are naturally explained by their correlated angular momenta due to similarities in their formation processes, most importantly the tidal shearing experienced by their host haloes (for a review on angular momentum models and intrinsic alignments, see [Schäfer 2009](#)).

Angular momentum is introduced into haloes in their formation as a consequence of tidal shearing which has been investigated

using perturbation theory, including the deformation of forming haloes, as well as by numerical studies ([Catelan 1995](#); [Catelan & Theuns 1996b,a](#); [Catelan et al. 2001](#); [Catelan & Porciani 2001](#); [Lee et al. 2007](#); [Codis et al. 2012](#)). There, the role of tidal torquing in the angular momentum build-up during galaxy formation is supported, but indicate that tidal torquing models might be predicting too high values for the amount of angular momentum ([Bullock et al. 2001](#); [Catelan & Porciani 2001](#); [Porciani et al. 2002a,b](#); [Hahn et al. 2007](#)) while perturbation theory seems to yield fairly reliable results for the angular momentum direction and explaining alignment effects of the halo with the ambient large-scale tidal field.

Angular momentum alignments give rise to a correlation in intrinsic ellipticities between neighbouring galaxies if the angular momentum direction of the galaxy corresponds to the one of the host halo. The scale of this correlation is predicted to be in the range of $\sim 1 \text{ Mpc}/h$ ([Crittenden et al. 2001](#); [Natarajan et al. 2001](#); [Schäfer & Merkel 2012](#)). Hence, intrinsic alignments influence the angular momentum correlation on small scales and can be of significance for high precision observations such as the future surveys mentioned above. Estimates of intrinsic alignment spectra arising from angular momentum based-models can be found in the works of [Croft & Metzler \(2000\)](#); [Crittenden et al. \(2001, 2002\)](#); [Mackey et al. \(2002\)](#). Due to their large complexity, [Schneider & Bridle](#)

^{*} e-mail: aram@ari.uni-heidelberg.de

(2010) devised a model which allows a much easier handling of intrinsic alignments.

Direct identification of the symmetry axis of the disc with the host halo angular momentum would lead to overestimation of the ellipticity alignments and is flawed as there might be large misalignments between these two vectors due to baryonic physics (Bailin et al. 2005; Stewart et al. 2013). Thus, we want to think of our ellipticity spectra as upper limits. Whereas the alignment model for spiral galaxies a quadratic dependency of the ellipticity on the tidal field is assumed (Crittenden et al. (2001)), elliptical galaxies follow a simpler linear alignment mechanism (Hirata & Seljak 2004). Sadly, the processes determining the orientation of the stellar disk inside a dark matter halo are not amenable to analytic calculations and even numerical simulations struggle to reach consensus about properties of galactic disks in a cosmological volume.

Intrinsic alignments are difficult to quantify (Godłowski 2012) but detections have been reported in a number of data sets, for instance in the Tully-catalogue (Pen et al. 2000), the Point Source Catalogue Redshift survey (Lee & Pen 2002), in the Sloan Digital Sky survey (Hirata et al. 2004; Mandelbaum et al. 2006; Lee & Pen 2007; Okumura & Jing 2009; Joachimi et al. 2011), in combination with the 2-degree Field Galaxy Redshift survey (Hirata et al. 2007) and the WiggleZ Dark Energy Survey (Mandelbaum et al. 2011), which allowed tests of alignment models (Blazek et al. 2011) and the determination of alignment model parameters. Mandelbaum et al. (2011) in particular provide a detailed description of the technical difficulties in measuring intrinsic correlations at redshifts relevant for gravitational lensing, and give fits for the intrinsic ellipticity correlation and the ellipticity-density cross-correlation. Some studies, however, remain sceptical about these detection reports (Andrae & Jahnke 2011).

As observations of galaxy ellipticities become increasingly precise, the study intrinsic alignments of galaxies based on angular momentum models will gain much interest in the future. Such models (Croft & Metzler 2000; Crittenden et al. 2001, 2002; Mackey et al. 2002) have been applied to estimate the significance of intrinsic alignments in the weak lensing convergence spectrum (Heavens et al. 2000; Heymans & Heavens 2003; Heymans et al. 2004) and bispectrum (Semboloni et al. 2008). Techniques for separating weak lensing data from intrinsic alignments range from discarding close galaxy pairs (King & Schneider 2002, 2003) to introducing a weighting in order to null out their contribution (Joachimi & Schneider 2008; Kitching & Taylor 2011), amplifying them relative to the weak lensing-induced correlations (King & Schneider 2003; Joachimi & Schneider 2010a,b; Joachimi & Bridle 2010) or to use the non-zero vortical modes (*B*-modes) of the intrinsic ellipticity field (Crittenden et al. 2002). With a model for intrinsic alignments at hand, it is of course possible to fit both the weak lensing ellipticity correlations and the intrinsic correlations at the same time, possibly constraining intrinsic alignment parameters (Bernstein 2009; Kirk et al. 2011) or use self-calibration techniques (Zhang 2010). Many of the removal techniques require very good control of redshift estimates (Bridle & King 2007) and can be extended to deal with cross-correlations between weak lensing and intrinsic alignments (King 2005). A puzzling result is that the contaminating effect of intrinsic alignments predicted from different angular momentum models in weak lensing data can be dramatically different. If intrinsic alignments are present in weak lensing data but not included in the model for the data when determining cosmological parameters, biases in the parameter estimates have to occur: Whereas Kirk et al. (2010, 2012) using a linear model found most

biases in the dark energy equation of state, Capranico et al. (2012) arrive at the conclusion that biases arise mostly in Ω_m and σ_8 .

Motivation for this paper is to study the influence of weak gravitational lensing on the observed ellipticity correlation, arising from the lensing effect of the intervening matter distribution. In order to assess the significance of intrinsic alignments in weak lensing measurements, Crittenden et al. (2001) found that the intrinsic signal is between 1 to 10 per cent of the measured lensing signal for a deep reaching survey. Here, our aim is to investigate the implications of the distortion (caused by weak gravitational shear) of galaxy ellipticities and the shift of galaxy positions by weak lensing on the shape of the *E*- and *B*-mode spectra of the lensed ellipticity correlation function. We will thus employ a formalism based on lensing of the cosmic microwave background (CMB) polarization (Seljak 1996; Hu & White 2001; Challinor & Lewis 2005; Lewis & Challinor 2006). It should be mentioned that in contrast to the lensing of the CMB where only the shifting effect is of importance and the polarization of the CMB photons remains unchanged, galaxy lensing involves also a distortion of ellipticities and a change of their orientation. In this regard, the analogy between the polarization of the CMB and the orientation of galaxy ellipticities has to be viewed differently. We use the model of Crittenden et al. (2001) for deriving a correlation function for the intrinsic ellipticities and apply the CMB formalism to it in order to observe characteristic features of weak lensing, such as the mixing of *E*- and *B*-modes. We expect a suppression of ellipticity correlations due to the shifting effect which dilutes and randomises the galaxy position at which ellipticities are measured.

In his paper we collect necessary results from cosmology, angular momentum generation in galaxies, ellipticity correlations, and weak lensing in Sect. 2, before describing in detail the formalism we use for computing lensed ellipticity spectra in Sect. 3, along with an investigation of the effects predicted by our formalisms for the case of a high- and a low-redshift galaxy sample. We summarise our main results in Sect. 4. As reference model we work with a basic spatially flat w CDM model with Gaussian adiabatic initial perturbations in cosmic density field. Model parameters were set to be $\Omega_m = 0.25$, $n_s = 1$, $\sigma_8 = 0.85$, $\Omega_b = 0.04$ and the Hubble-radius $c/H_0 = 2996.9$ Gpc/h, with $h = 0.72$. The dark energy equation of state parameter w was assumed to be constant at a value of -0.9 .

2 COSMOLOGY

2.1 Dark energy cosmologies

The time evolution of isotropic Friedmann-universe with homogeneous dark matter and dark energy is described by the Hubble function $H(a) = d \ln a / dt$, which is given by

$$\frac{H^2(a)}{H_0^2} = \frac{\Omega_m}{a^3} + (1 - \Omega_m) \exp\left(3 \int_a^1 d \ln a (1 + w(a))\right), \quad (1)$$

with the matter density parameter Ω_m and the dark energy equation of state function $w(a)$. Spatial flatness requires the dark energy density to be $1 - \Omega_m$. The comoving distance χ can be computed from the scale factor a ,

$$\chi = c \int_a^1 \frac{da}{a^2 H(a)}. \quad (2)$$

For the galaxy redshift distribution $n(z)dz$, we use a standard shape

$$n(z) = n_0 \left(\frac{z}{z_0}\right)^2 \exp\left(-\left(\frac{z}{z_0}\right)^\beta\right) dz \quad \text{with} \quad \frac{1}{n_0} = \frac{z_0}{\beta} \Gamma\left(\frac{3}{\beta}\right), \quad (3)$$

with $\beta = 3/2$. We choose z_0 such that the distribution has a median redshift of 0.9 corresponding to EUCLID (Amara & Réfrégier 2007) which we contrast with a galaxy distribution of identical shape but with a much lower median of 0.3. We will refer to the two application cases as the high and low redshift galaxy sample, respectively. The distribution can be rewritten in terms of comoving distance using the relation $p(z)dz = p(\chi)d\chi$ with $dz/d\chi = H(\chi)/c$.

2.2 CDM power spectrum

The statistical properties of the overdensity field δ is in the case of homogeneous, isotropic and Gaussian fluctuations described by the spectrum $P_\delta(k)$. Inflationary models suggest the ansatz

$$P_\delta(k) \propto k^{n_s} T^2(k), \quad (4)$$

with the transfer function $T(k)$. This function is approximated by

$$T(q) = \frac{\ln(1 + 2.34q)}{2.34q} M(q)^{-\frac{1}{4}}, \quad (5)$$

(see Bardeen et al. 1986), with the polynomial

$$M(q) = 1 + 3.89q + (16.1q)^2 + (5.46q)^3 + (6.71q)^4 \quad (6)$$

The transfer function depends most strongly on the parameters Ω_m and h which form the shape-parameter Γ ,

$$\Gamma = \Omega_m h \exp\left(-\Omega_b \left[1 + \frac{\sqrt{2}h}{\Omega_m}\right]\right), \quad (7)$$

and shows slight corrections due to the baryon density Ω_b Sugiyama (1995). With Γ , the wave vector k is scaled according to $q = k/\Gamma$. The linearly evolved spectrum $P(k)$ is normalised to show the variance σ_8^2 on a comoving scale of $R = 8 \text{ Mpc}/h$,

$$\sigma_R^2 = \int \frac{k^2 dk}{2\pi^2} P_\delta(k) W^2(kR) \quad (8)$$

with a Fourier transformed spherical top hat filter function, $W(x) = 3j_1(x)/x$. $j_\ell(x)$ is the spherical Bessel function of the first kind of order ℓ (Abramowitz & Stegun 1972). Weak lensing spectra will be computed for both linear and nonlinear structures, for the latter we employ the extension of $P(k)$ to nonlinear structure formation proposed by Smith et al. (2003). In the limit of small perturbations $|\delta| \ll 1$, cosmic structure formation is linear and homogeneous, $\delta(\mathbf{x}, a) = D_+(a)\delta(\mathbf{x}, a=1)$. The time evolution of the cosmic density field is then given by the growth function $D_+(a)$, that follows from the growth equation (Turner & White 1997; Wang & Steinhardt 1998; Linder & Jenkins 2003),

$$\frac{d^2}{da^2} D_+(a) + \frac{1}{a} \left(3 + \frac{d \ln H}{d \ln a}\right) \frac{d}{da} D_+(a) = \frac{3}{2a^2} \Omega_m(a) D_+(a), \quad (9)$$

such that the spectrum $P(k) \propto D_+^2(a)$, while the nonlinear extension to $P(k)$ has its own parametrised time evolution based on $\Omega_m(a)$,

$$\frac{\Omega_m(a)}{\Omega_m} = \frac{1}{a^3} \frac{H_0^2}{H^2(a)}, \quad (10)$$

which can be derived from the adiabaticity of the cosmic fluids.

2.3 Angular momentum from tidal shearing

Angular momentum generation in CDM-haloes is a Lagrangian perturbative process (Hoyle 1949; Sciamia 1955; Peebles 1969; Doroshkevich 1970; White 1984): The variation of velocities displacing a protogalactic region acts as a torque which generates angular momentum L_α :

$$L_\alpha = a^3 H(a) \frac{dD_+}{da} \epsilon_{\alpha\beta\gamma} I_{\beta\delta} \Phi_{,\delta\gamma}, \quad (11)$$

with the tidal shear being defined as the Hessian of the gravitational potential and the inertia tensor measuring the second moments of the mass distribution inside the protohalo,

$$\Phi_{,\delta\gamma} \equiv \frac{\partial^2 \Phi}{\partial x_\delta \partial x_\gamma} \quad \text{and} \quad (12)$$

$$I_{\beta\delta} \equiv \Omega_m \rho_{\text{crit}} \int d^3 q \delta(q) (q - \bar{q})_\beta (q - \bar{q})_\delta, \quad (13)$$

respectively, with implicit summation over repeated indices. \mathbf{q} are Lagrangian coordinates moving along with the halo's centre of gravity $\bar{\mathbf{q}}$. Note that the second moments of the mass distribution $I_{\beta\delta}$ is referred to as the inertia tensor despite the fact that it has a different ordering of the axes.

This relation reflects the interesting requirement of misalignments between the shear and inertia eigensystems which is necessary for angular momentum generation: Only the antisymmetric tensor $X_{\beta\gamma}^- = \sum_\delta (I_{\beta\delta} \Phi_{,\delta\gamma} - \Phi_{,\beta\delta} I_{\delta\gamma})/2$ is relevant for the angular momentum (Schäfer & Merkel 2012), $L_\alpha \propto X_{\beta\gamma}^-$, because the contraction of the symmetric contribution $X_{\beta\gamma}^+$ with the antisymmetric $\epsilon_{\alpha\beta\delta}$ vanishes. The antisymmetric tensor X_- is equal to the commutator $[I_{\beta\delta}, \Phi_{,\delta\gamma}]$ which suggests that the tidal shear and the inertia are not allowed to be simultaneously diagonalisable and must not have a common eigensystem, otherwise angular momentum can not arise.

In this work we use the angular momentum-based ellipticity correlation model proposed by Crittenden et al. (2001). There, ellipticities are set into relation to tidal shear by means of a conditional probability distribution $p(\mathbf{L}|\Phi_{,\alpha\beta})d\mathbf{L}$. Such a distribution has been proposed by Lee & Pen (2001) as being Gaussian with the covariance

$$\text{cov}(L)_{\alpha\beta} \propto \frac{1}{3} \left(\frac{1+a}{3} \delta_{\alpha\beta} - a (\hat{\Phi}^2)_{\alpha\beta} \right), \quad (14)$$

which acquires a dependence on the tidal shear tensor, that has been normalised and made trace-free, $\text{tr}(\hat{\Phi}) = 0$ and $\text{tr}(\hat{\Phi}^2) = 1$. In this way, the variance of the angular momentum field varies with the tidal shear, and the randomness of the angular momentum field is controlled by the misalignment parameter a , which describes the average orientation of the protohalo's inertia to the tidal shear eigensystem. a has been measured in numerical simulation to be the value ≈ 0.25 , and we will use this value in this work.

This description is valid on scales where the correlations between inertia tensors are negligible and is sufficient because we are only interested in the angular momentum direction, as will be explained in the next section. Therefore, one does not need the variance $\langle L^2 \rangle$ of the angular momentum field as a parameter and it is possible to marginalise the distribution over the magnitude L ,

$$p(\hat{\mathbf{L}}|\Phi_{,\alpha\beta}) = \int L^2 dL p(\mathbf{L}|\Phi_{,\alpha\beta}). \quad (15)$$

In this picture correlations between angular momenta can be traced back to correlations between tidal shears that neighbouring galaxies experienced in building up their angular momenta. It should be noted, however, that recent investigations provide evidence that the nonlinear evolution of galactic angular momenta can be vorticity driven (Libeskind et al. 2012; Lee 2013) as an alternative to tidal torquing.

2.4 Intrinsic ellipticity correlations

We assume that the halo angular momentum axis and the symmetry axis of the galactic disk are parallel. The tilting of the disk relative to the line of sight determines the aspect ratio under which the galactic disk is viewed and therefore the galaxy's ellipticity. In this way, the angular momentum direction $\hat{L} = \mathbf{L}/L$ with $L = |\mathbf{L}|$ determines the ellipticity ϵ . In this picture, ellipticity correlations are derived from angular momentum direction correlations and ultimately from tidal shear correlations (Heavens et al. 2000; Crittenden et al. 2001, 2002; Mackey et al. 2002; Heymans & Heavens 2003). Specifically, the two components of the ellipticity field can be combined to form the complex ellipticity with ϵ_+ as the real and ϵ_\times as the complex part, and related to the angular momentum direction \hat{L} :

$$\epsilon = \epsilon_+ + i\epsilon_\times \quad \text{with} \quad \epsilon_+ = \alpha \frac{\hat{L}_x^2 - \hat{L}_y^2}{1 + \hat{L}_z^2}, \quad \epsilon_\times = 2\alpha \frac{\hat{L}_x \hat{L}_y}{1 + \hat{L}_z^2}, \quad (16)$$

when the coordinate system is aligned with its z -axis parallel to the line of sight. Under a rotation of the coordinate frame by an angle φ the complex ellipticity transforms according to the relation $\epsilon \rightarrow \exp(2i\varphi)\epsilon$, in accordance with the spin-2 property of the ellipticity field. α is the disk thickness parameter and can be used for describing a weaker dependence of ϵ on \hat{L} if the galactic disk has a finite thickness. We use the numerical value $\alpha = 0.75$ which has been measured in the APM galaxy sample by Crittenden et al. (2001).

Linking the ellipticity components ϵ_+ and ϵ_\times to the angular momentum direction \hat{L} and ultimately to the tidal shear tensor by means of the conditional probability density $p(\mathbf{L}|\Phi_{,\alpha\beta})d\mathbf{L}$ provides means to derive ellipticity correlations in terms of tidal shear correlations, and ultimately as functions of the CDM-spectrum. Because we are interested in ellipticity correlations of galaxies, we smooth the CDM-spectrum with a Gaussian filter on the mass-scale $3 \times 10^{11} M_\odot/h$. In this way, one can write down a 3-dimensional correlation function of the ellipticity field as a function of moments $\zeta_n(r)$ (see Crittenden et al. 2001) of the CDM-spectrum and finally to carry out a Limber projection for obtaining the angular correlation function of the ellipticity field. The correlation function can be Fourier-transformed to yield the E -mode and B -mode ellipticity spectra (c.f. Sect. 2.7). The related model proposed by Mackey et al. (2002) yields very similar shapes for the ellipticity spectra but predicts smaller amplitudes.

2.5 Weak gravitational lensing

The lensing potential ψ is defined as the line of sight projected gravitational potential Φ

$$\psi = \int_0^{\chi_H} d\chi \frac{G(\chi)}{\chi} \Phi, \quad (17)$$

with the lensing-efficiency weighted galaxy distribution $G(\chi)$ as a weighting function,

$$G(\chi) = \int_\chi^{\chi_H} d\chi' n(\chi') \left(1 - \frac{\chi}{\chi'}\right) \quad (18)$$

The lensing deflection angle α is obtained from the lensing potential ψ by differentiation, $\alpha_i = \partial_i \psi$. Further differentiation yields the projected tidal field $\psi \equiv \partial_i \partial_j \psi$ which can be decomposed with the Pauli-matrices σ_α , because they constitute a basis for the vector space of 2×2 matrices,

$$\psi = \sum_{\alpha=0}^3 a_\alpha \sigma_\alpha = (1 - \kappa)\sigma_0 - \gamma_+ \sigma_1 - \gamma_\times \sigma_3, \quad (19)$$

(c.f. Abramowitz & Stegun 1972; Arfken & Weber 2005), where σ_0 denotes the 2-dimensional unit matrix. For $\alpha = 1, 2, 3$, the Pauli-matrices have the properties $\sigma_\alpha^2 = \sigma_0$ and $\text{tr}(\sigma_\alpha) = 0$. Due to the property $\sigma_\alpha \sigma_\beta = \sigma_0 \delta_{\alpha\beta} + i\epsilon_{\alpha\beta\gamma} \sigma_\gamma$ of the Pauli-matrices, the coefficients a_α can be recovered by using $a_\alpha = \frac{1}{2} \text{tr}(\psi \sigma_\alpha)$. In particular, one identifies the weak lensing convergence $\kappa = \frac{1}{2} \text{tr}(\psi \sigma_0)$ with the unit matrix σ_0 and the two components of shear $\gamma_+ = \frac{1}{2} \text{tr}(\psi \sigma_1)$ and $\gamma_\times = \frac{1}{2} \text{tr}(\psi \sigma_3)$. The standard expression for κ can be recovered with $\kappa = \frac{1}{2} \text{tr}(\psi \sigma_0) = \frac{1}{2} \sum_i \partial_i \partial_i \psi = \frac{1}{2} \Delta_\theta \psi = \frac{1}{2} \text{div}_\theta \alpha$ with the deflection angle $\alpha = \nabla_\theta \psi$.

The two components of lensing shear are combined to form the complex shear $\gamma = \gamma_+ + i\gamma_\times$ with the transformation property $\gamma \rightarrow \gamma \exp(2i\varphi)$ under a rotation of the coordinate frame by an angle φ . Violations of the symmetry of ψ are very small and might e.g. be caused by geodesic effects such as lens-lens-coupling and Born-corrections (see Shapiro & Cooray 2006; Cooray & Hu 2002; Krause & Hirata 2009; Bernardeau et al. 2010, for a detailed computation). Therefore, an expansion coefficient for the contribution due to σ_2 which parametrises image rotation was neglected. In the limit of weak lensing, the galaxy ellipticity is transformed according to $\epsilon \rightarrow \epsilon + \gamma$.

2.6 Spectrum of the weak lensing potential

The spectrum of the weak lensing potential follows from substituting the line of sight-expression $\psi = \int d\chi G(\chi)/\chi \Phi$ into the Limber-equation (Limber 1954),

$$C_\psi(\ell) = \int_0^{\chi_H} \frac{d\chi}{\chi^4} G(\chi)^2 P_\Phi(k = \ell/\chi, a(\chi)), \quad (20)$$

where we used the most basic flat-sky description. The power spectrum $P_\Phi(k, a)$ of the gravitational potential Φ at the scale-factor a follows from the comoving Poisson equation $\Delta\Phi = 3H_0^2 \Omega_m / (2a)\delta$ and is related to the density power spectrum $P_\delta(k, a)$ by

$$P_\Phi(k, a) = \left(\frac{3\Omega_m}{2} \frac{D_+(a)}{a} \right)^2 \frac{P_\delta(k)}{(\chi_H k)^4}, \quad (21)$$

with the Hubble distance $\chi_H = c/H_0$ making the k^{-4} -factor dimensionless. By differentiation one obtains the spectrum $C_\alpha(\ell) = \ell^2 C_\psi(\ell)$ of the deflection angle $\alpha = \nabla_\theta \psi$ and the spectrum $C_\kappa(\ell) = \ell^4 / 4 C_\psi(\ell)$ of the weak lensing convergence $\kappa = \frac{1}{2} \text{div}_\theta \alpha = \frac{1}{2} \Delta_\theta \psi$, which is equal to the E -mode correlation function $C_E^\gamma(\ell)$ of the weak lensing shear γ in the absence of $C_B^\gamma(\ell)$ (c.f. the following section).

The angular spectrum $C_\psi(\ell)$ of the weak lensing potential ψ resulting from the Limber-projection of $P_\Phi(k)$ is depicted in Fig. 1 along with the spectrum $C_\alpha(\ell)$ of the lensing deflection angle α and the weak lensing shear spectrum $C_E^\gamma(\ell)$, for the high redshift galaxy sample with $z_{\text{med}} = 0.9$ and the low redshift galaxy sample with $z_{\text{med}} = 0.3$. Furthermore, predictions for the spectra using a linear and a nonlinear CDM-spectrum $P(k)$ are contrasted.

2.7 Correlations of spin-2 fields

Both the galaxy ellipticities and the Stokes-parameters of the CMB-polarisation form a tensorial spin-2 field, which means that rotations of the coordinate frame by an angle φ give rise to a transformation of the tensor components as $\epsilon \rightarrow \exp(2i\varphi)\epsilon$ and $P \rightarrow \exp(2i\varphi)P$, when the ellipticity is written as a complex ellipticity

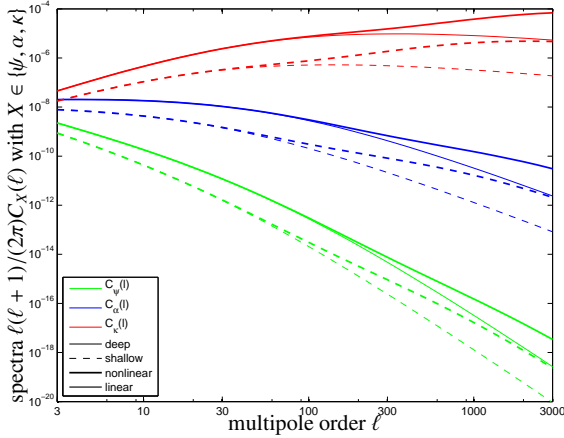


Figure 1. Angular spectrum $C_\psi(\ell)$ (green line) of the lensing potential ψ , the spectrum $C_\alpha(\ell) \equiv \ell^2 C_\psi(\ell)$ (blue line) of the lensing deflection field $\alpha = \nabla_\perp \psi$ and the spectrum $C_\kappa(\ell) = \ell^4/4 C_\psi(\ell)$ of the E -mode shear, for the high redshift galaxy sample (solid lines) and the low redshift galaxy sample (dashed lines), comparing the prediction for a linear CDM spectrum (thin lines) with a nonlinear one (thick lines).

$\epsilon = \epsilon_+ + i\epsilon_\times$ and the polarisation tensor P is composed of the Stokes parameters Q and U according to $P = U + iQ$.

Correlations between two points θ_1 and θ_2 separated by the distance θ of a spin-2 field such as the complex polarisation $P = Q + iU$, the complex ellipticity $\epsilon = \epsilon_+ + i\epsilon_\times$ or the weak lensing shear $\gamma = \gamma_+ + i\gamma_\times$ are described in terms of two functions $\xi_\pm(\theta)$,

$$\xi_+(\theta) = \langle \epsilon_+(\theta_1) \epsilon_+(\theta_2) \rangle + \langle \epsilon_\times(\theta_1) \epsilon_\times(\theta_2) \rangle, \quad (22)$$

$$\xi_-(\theta) = \langle \epsilon_+(\theta_1) \epsilon_-(\theta_2) \rangle - \langle \epsilon_\times(\theta_1) \epsilon_\times(\theta_2) \rangle. \quad (23)$$

The correlation functions $\xi_\pm(\theta)$ are constructed from the variances of the components ϵ_+ and ϵ_\times using vanishing cross-correlations, $\langle \epsilon_+ \epsilon_\times \rangle = 0$. They can be transformed to the spectra $C_E^\epsilon(\ell)$ and $C_B^\epsilon(\ell)$ of the gradient (E) and vorticity (B) modes of the ellipticity field,

$$C_E^\epsilon(\ell) = \pi \int \theta d\theta [\xi_+(\theta) J_0(\ell\theta) + \xi_-(\theta) J_4(\ell\theta)], \quad (24)$$

$$C_B^\epsilon(\ell) = \pi \int \theta d\theta [\xi_+(\theta) J_0(\ell\theta) - \xi_-(\theta) J_4(\ell\theta)], \quad (25)$$

by Fourier transform (Kaiser 1992; Schneider et al. 2002; Schneider & Kilbinger 2007; Fu & Kilbinger 2010). Completely analogous formulae apply for the description of the angular correlation properties of the weak lensing shear and their transformation to Fourier space yielding $C_E^\gamma(\ell)$ and $C_B^\gamma(\ell)$, the latter of which is zero if lensing on a scalar gravitational potential is considered and if the Born-approximation applies.

Figs. 4 and 5 shows intrinsic ellipticity spectra $C_E^\epsilon(\ell)$ and $C_B^\epsilon(\ell)$ for the EUCLID galaxy sample with its median redshift at $z_{\text{med}} = 0.9$ which are contrasted with the spectra $C_E^\epsilon(\ell)$ and $C_B^\epsilon(\ell)$ for a galaxy sample with a much lower median redshift of $z_{\text{med}} = 0.3$. For comparison, we superpose the corresponding spectra $C_E^\gamma(\ell)$ for the weak lensing shear γ measured on the same galaxy populations, both for a linear and a nonlinear CDM-spectrum.

The spectra are constant and equal in amplitude up to multipoles of $\ell \simeq 100$, indicating the absence of correlations such that on each scale on measures the variance of the uncorrelated ellipticity field. Correlations become important on angular scales $\ell \gtrsim 300$ where the spectra level off and decrease from multipoles

of $\ell \gtrsim 3000$ on very rapidly. In the peak region, the ellipticity E -modes have an amplitude larger than the B -modes by about an order of magnitude. Consistent with expectations the lensing spectrum exceeds intrinsic ellipticity correlations significantly for the high redshift case, but one observes the contrary behaviour for the low redshift case. Furthermore, the impact of nonlinear structure formation is stronger in the low-redshift case, as non-linearities had more time to develop.

3 IMPRINTS ON LENSING ON ELLIPTICITIES

3.1 Lensing effects on ellipticity fields

In weak lensing studies it is commonly assumed that the observed lensed galaxies would have had no shape-correlations without lensing, and that there is no clustering in the galaxy sample, neither along the line-of-sight nor perpendicular to it. In short, intrinsic ellipticities are drawn independently from a distribution which is commonly assumed to be Gaussian with variance σ_ϵ^2 . In the estimation process of weak lensing spectra from galaxy shapes the intrinsic shape variations would contribute the Poissonian term σ_ϵ^2/n , if the estimation process comprises n galaxies.

The physical picture we have in mind is a background field of intrinsically correlated ellipticities on which gravitational lensing acts by deflection and shear, while there are no correlations between the ellipticities and the matter distribution responsible for lensing. In this sense, we consider lensing on II-alignments, while neglecting GI-alignments, which vanish in the case of Gaussian fluctuations statistics for quadratic alignment models as the one used in this work, but would be present in nonlinear structures (Lee & Pen 2008). Other lensing-induced effects are modulations in the surface density of galaxies, due to the interplay between magnification of the image brightness and dilution over a larger solid angle, which we neglect for the purpose of this paper.

3.2 Adaptation of the CMB-lensing formalism

As in the case of CMB lensing where the (complex) polarisation tensor $P(\theta) = Q(\theta) + iU(\theta)$ is measured at a new position $\theta + \alpha$ due to gravitational lensing, we assert that the ellipticity ϵ is not observed at the true position θ of the galaxy, but at the apparent position $\theta + \alpha$, $\epsilon(\theta) \rightarrow \epsilon(\theta + \alpha)$ with the lensing deflection angle α . Additionally, a variation of the deflection angle across the galaxy image leads to a distortion described by the complex shear γ and the convergence κ .

Adapting the CMB-lensing formalism, correlations between the components of the shifting angle α at two positions θ_1 and θ_2 are described by (Seljak 1996)

$$\langle \alpha_i(\theta_1) \alpha_j(\theta_2) \rangle = \frac{1}{2} C_0(\theta) - C_2(\theta) \hat{\theta}_i \hat{\theta}_j \quad (26)$$

with $\theta = \theta_2 - \theta_1$. The two correlation functions of the deflection angle are defined as

$$C_0(\theta) = \int \frac{\ell^3 d\ell}{2\pi} C_\psi(\ell) J_0(\ell\theta) \quad (27)$$

and

$$C_2(\theta) = \int \frac{\ell^3 d\ell}{2\pi} C_\psi(\ell) J_2(\ell\theta). \quad (28)$$

We abbreviate the variance of the deflection angle

$$\sigma^2(\theta) = C_0(0) - C_0(\theta) \quad (29)$$

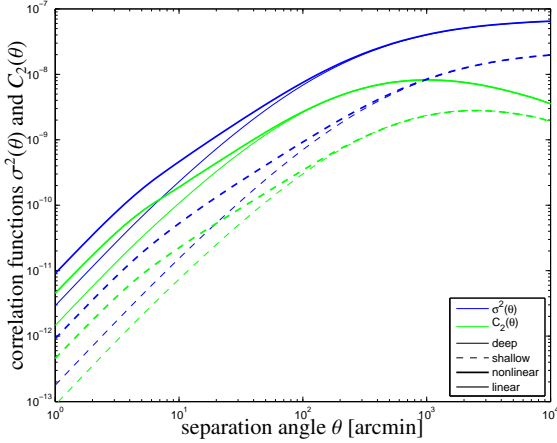


Figure 2. Correlation functions $\sigma^2(\theta) = C_0(0) - C_0(\theta)$ (blue line) and $C_2(\theta)$ (green line) as a function of separation angle θ , for the high redshift galaxy sample (solid line) and the low redshift galaxy sample (dashed line), again comparing the predictions from linear (thin lines) and nonlinear (thick lines) CDM spectra.

in complete analogy to CMB-lensing for describing uncorrelated deflections.

The characteristic function of α , i.e. the Fourier transform of the probability density $p(\alpha)d\alpha$ is then obtained as:

$$\langle \exp(i\ell[\alpha(\theta_1) - \alpha(\theta_2)]) \rangle = \exp\left(\frac{\ell^2}{2}[-\sigma^2(\theta) + \cos 2\varphi_\ell C_2(\theta)]\right), \quad (30)$$

and can be expressed in the case of Gaussian distributions in terms of $\sigma^2(\theta)$ and $C_2(\theta)$. In the case of CMB-lensing, non-Gaussian contributions have been shown to have negligible effect on the deflection angle statistics (Carbone et al. 2009; Merkel & Schäfer 2011) and in the case of weak cosmic shear, arguments about the rarity of strong deflections not described by a Gaussian distributions apply in a similar way (Hamana et al. 2005).

Fig. 2 shows the quantities $\sigma^2(\theta) = C_0(0) - C_0(\theta)$ and $C_2(\theta)$ needed in this formalism, for both a high and a low redshift galaxy sample and for linear and nonlinear CDM-spectra: Both correlation functions assume larger values for the high-redshift sample and for lensing on nonlinear structures, which in particular causes a larger variance of the deflection angle on small angular scales. For large values of the argument θ , both correlation function start to oscillate rapidly.

The correlation properties of the lensing-distorted ellipticity field can be described using the two correlation functions $\xi_\pm(\theta)$,

$$\xi_+(\theta) = \langle \epsilon^*(\mathbf{x} + \alpha)\epsilon(\mathbf{x}' + \alpha') \rangle \quad (31)$$

$$\xi_-(\theta) = \langle \exp(-4i\phi_\ell)\epsilon(\mathbf{x} + \alpha)\epsilon(\mathbf{x}' + \alpha') \rangle. \quad (32)$$

Substituting the correlation function for the deflection angle in the Fourier-transforms of the above expressions yields the correlation functions $\xi'_\pm(\theta)$ of the new ellipticity field. They can be transformed to E -mode and B -mode spectra with the standard transformations eqns. (24) and (25).

These steps lead to a transformation formula the E -mode and B -mode spectra of the ellipticity field, which can be summarised by a concise matrix notation:

$$\begin{pmatrix} C'_E(\ell) \\ C'_B(\ell) \end{pmatrix} = \int \ell' d\ell' \begin{pmatrix} W_+(\ell, \ell') & W_-(\ell, \ell') \\ W_-(\ell, \ell') & W_+(\ell, \ell') \end{pmatrix} \begin{pmatrix} C_E(\ell') \\ C_B(\ell') \end{pmatrix}. \quad (33)$$

This notation shows explicitly the mixing between scales due to the convolution weighted with $W_+(\ell, \ell')$ and the conversion between $C_E^\epsilon(\ell)$ and $C_B^\epsilon(\ell)$ under the influence of $W_-(\ell, \ell')$. And clearly, the displacement mechanism can not generate ellipticity correlations as $C'_X(\ell)$ remains zero if the $C_X^\epsilon(\ell)$ is zero to begin with, $X \in \{E, B\}$.

These kernels $W_\pm(\ell, \ell')$ are given by

$$W_+(\ell, \ell') = \frac{1}{2} \int \theta d\theta [J_0(\ell\theta)A(\ell', \theta) + J_4(\ell\theta)B(\ell', \theta)], \quad (34)$$

$$W_-(\ell, \ell') = \frac{1}{2} \int \theta d\theta [J_0(\ell\theta)A(\ell', \theta) - J_4(\ell\theta)B(\ell', \theta)], \quad (35)$$

with the functions

$$A(\ell, \theta) = \exp\left(-\frac{\ell^2 \sigma^2(\theta)}{2}\right) \left[J_0(\ell, \theta) + \frac{\ell^2}{2} C_2(\theta) J_4(\ell\theta) \right], \quad (36)$$

$$B(\ell, \theta) = \exp\left(-\frac{\ell^2 \sigma^2(\theta)}{2}\right) \left[J_4(\ell, \theta) + \frac{\ell^2}{2} C_2(\theta) J_0(\ell\theta) \right]. \quad (37)$$

Here, uncorrelated deflections contained in the variance $\sigma^2(\theta)$ give rise to a Gaussian convolution kernel while correlated deflections due to $C_2(\theta)$ show a more complicated mode-coupling. We abbreviated $J_s(x) = J_2(x) + J_6(x)$.

In the limit absent lensing, $C_0(\theta) = C_2(\theta) = 0$ such that $W_+(\ell, \ell') = \delta(\ell - \ell')/\ell$ and $W_-(\ell, \ell') = 0$, due to the orthogonality relations of the cylindrical Bessel functions,

$$\int (\ell\theta) d\theta J_n(\ell\theta)J_n(\ell'\theta) = \delta_D(\ell - \ell'). \quad (38)$$

In this case, the convolution is reduced to a Dirac δ_D -function and the mixing matrix is the unit matrix, so that the E -mode and B -mode amplitudes are conserved and there is no convolution between ℓ -modes. We have verified that higher-order corrections arising in the transformation of correlation functions do have a negligible effect for the evolved ellipticity correlations (Challinor & Lewis 2005; Lewis & Challinor 2006) and in our numerical implementation, we used the same relations for the required number of grid points ($4 \times \ell_{\max}$ tabulated values of $\sigma^2(\theta)$ and $C_2(\theta)$ in θ) as suggested for CMB-lensing.

3.3 Conversion between E and B -modes

Fig. 3 shows the mode coupling kernels $W_+(\ell, \ell')$ and $W_-(\ell, \ell')$ for the high-redshift distribution and computed for a nonlinear CDM spectrum, with qualitatively very similar results for the low redshift sample. Apart from a smooth variation of $W_+(\ell, \ell')$, which acts on the ellipticity spectra by convolution, one notices tall spikes at $\ell = \ell'$, illustrating the closeness to diagonality of the W_+ -matrix. In contrast, $W_-(\ell, \ell')$ shows smaller amplitudes by about two orders of magnitude, indicating that the conversion between E - and B -modes is a minor effect compared to the convolution mediated by $W_+(\ell, \ell')$, with strong oscillatory features close to diagonal $\ell = \ell'$. The kernels $W_\pm(\ell, \ell')$ show an inverse scaling with multipole ℓ such that they become approximately constant when substituted into the relation (33) by multiplication with the $\ell' d\ell'$ -differential.

3.4 Lensed ellipticity spectra

The final results are given in Figs. 4 and 5, which compare the initial ellipticity spectra $C_E^\epsilon(\ell)$ and $C_B^\epsilon(\ell)$ of the ellipticity field as predicted by correlated angular momenta, and the distorted spectra $C'_E(\ell)$ and $C'_B(\ell)$ that encapsulate the imprint of lensing deflection and therefore display altered correlation properties. For comparison

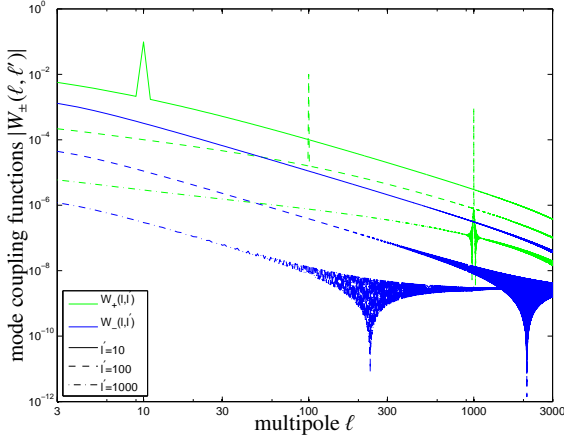


Figure 3. Mode coupling functions $W_+(\ell, \ell')$ (green lines) and $W_-(\ell, \ell')$ (blue lines) used in the transformation of the ellipticity spectra, which describes the convolving effect on the ellipticity spectra, for $\ell' = 10, 100, 1000$ (solid, dashed and dash-dotted, respectively). The coupling functions shown are the ones for the high redshift galaxy sample, while those for the low redshift sample look qualitatively very similar.

with weak lensing, we plot the weak convergence spectrum $C_\kappa(\ell)$ expected from the EUCLID galaxy sample in comparison, for a nonlinear CDM spectrum (using the parametrisation by [Smith et al. 2003](#)).

The first observation is that ellipticity correlations reach amplitudes similar to those of the weak lensing convergence in the nonlinear part corresponding to amplitudes $\ell \lesssim 300$, and that the intrinsic E -mode spectrum $C_E^\epsilon(\ell)$ is larger than the B -mode spectrum $C_B^\epsilon(\ell)$ by about an order of magnitude in this regime. On larger angular scales, there are no appreciable ellipticity correlations and one effectively observes the variance of the ellipticity field for uncorrelated objects. Consequently, the spectra have identical amplitudes and are effectively constant. In this regime, the shifting effect is not able to affect the galaxies, which is a well-known result in CMB-lensing, where scale free-spectra are invariant ([Lewis & Challinor 2006](#)): The mode-conversion mechanism is ineffective if the spectra are equal, $C_E^\epsilon(\ell) = C_B^\epsilon(\ell)$, and the convolution with $W_+(\ell, \ell')$ is not able to redistribute amplitudes. In contrast, both spectra are affected on multipoles $\ell > 1000$, where in particular $C_B^\epsilon(\ell)$ has decreased relative to $C_B^\epsilon(\ell)$.

Fig. 6 shows the changes in the spectra as a function of multipole ℓ by giving the ratio of the evolved and initial E -mode and B -mode spectra, $C_E^\epsilon(\ell)/C_E^\epsilon(\ell)$ and $C_B^\epsilon(\ell)/C_B^\epsilon(\ell)$ respectively. As already indicated by Figs. 4 and 5, we see a significant decrease of amplitude amounting to 5% for the E - and 30% for the B -modes from $\ell = 3000$ on in the case of the high-redshift sample and from $\ell = 1000$ on in the case of the low-redshift sample. This implies that for EUCLID's weak lensing application, changes in the ellipticity spectra are affecting scales where the shape noise starts dominating, but for shallower surveys, lower multipoles would be affected by weak lensing deflection. We conclude that in the case of deep surveys such as EUCLID, weak lensing manifests itself primarily as weak lensing shear which dominates over intrinsic alignments and the lensing deflection effect shapes intrinsic alignments by decreasing their amplitudes only at very high multipoles.

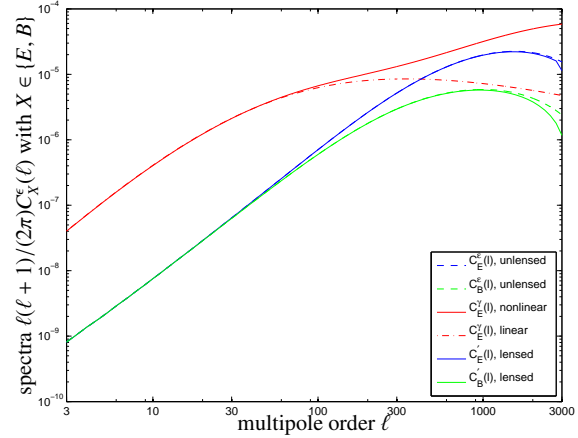


Figure 4. Ellipticity spectra $C_E^\epsilon(\ell)$ (blue line) and $C_B^\epsilon(\ell)$ (green line) as predicted by the angular momentum model (dashed lines), and the lensed ellipticity spectra (solid lines) where the deflections were computed for the high redshift galaxies. For comparison, we plot the spectrum $C_E^\gamma(\ell)$ of the weak lensing shear γ (red line).

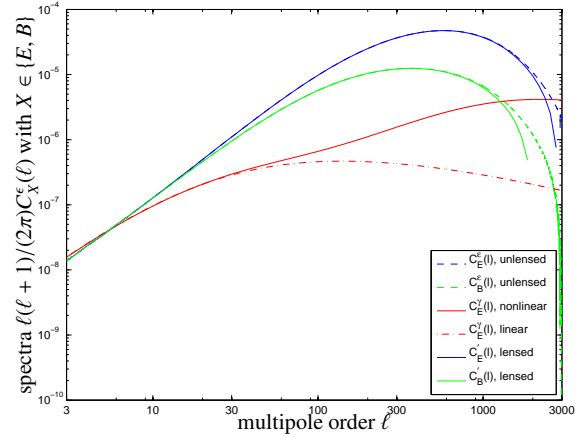


Figure 5. Ellipticity spectra $C_E^\epsilon(\ell)$ (blue line) and $C_B^\epsilon(\ell)$ (green line) as predicted by the angular momentum model (dashed lines), and the lensed ellipticity spectra (solid lines) where the deflections were computed for the low redshift galaxies. For comparison, we plot the spectrum $C_E^\gamma(\ell)$ of the weak lensing shear γ for the same galaxy sample (red line).

3.5 Violated homogeneity of the ellipticity field

Lensing of the intrinsic ellipticity field introduces a violation of their statistical homogeneity in complete analogy to the lensing deflection acting on the CMB polarisation. For a given realisation of the deflection potential ψ one can estimate the lensing effect on the ellipticity spectra, $X = E, B$:

$$\langle \epsilon_X'(\ell) \epsilon_X'(\ell') \rangle = f_X(\ell, \ell') \psi(\ell - \ell') \quad (39)$$

with

$$f_E(\ell, \ell') = (\ell - \ell') [\ell C_E^\epsilon(\ell) + \ell' C_E^\epsilon(\ell')] \cos 2\varphi_{\ell, \ell'} \quad (40)$$

$$f_B(\ell, \ell') = (\ell - \ell') [\ell C_B^\epsilon(\ell) + \ell' C_B^\epsilon(\ell')] \cos 2\varphi_{\ell, \ell'} \quad (41)$$

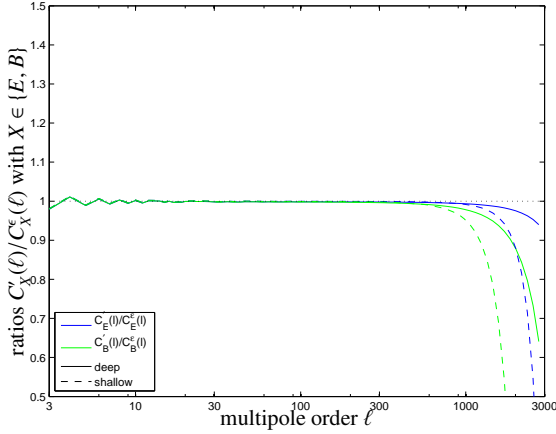


Figure 6. Ratios $C'_E(\ell)/C^\epsilon_E(\ell)$ (blue lines) and $C'_B(\ell)/C^\epsilon_B(\ell)$ (green lines), for both a high redshift galaxy sample (solid lines) and a low redshift galaxy sample (dashed lines).

where $\varphi_{\ell,\ell'}$ the enclosed angle. Nonzero correlations between multipoles are the signature of homogeneity violation introduced by a single realisation and they would disappear in the process of ensemble averaging the lensing potential.

In order to place an upper limit on this effect we select a particularly simple geometry, namely parallel alignment of the wave vectors ℓ and ℓ' such that the cosines are equal to one and have the wave vectors then differ by one unit, $\ell - \ell' = 1$, as the coupling between neighbouring multipoles is strongest due to the rapid decline of the lensing potential's Fourier transform with increasing ℓ . In this limit, and if one assumes the ellipticity spectra to be slowly varying, the ratio between the off-diagonal and diagonal correlations is given by

$$\frac{C'_E(\ell, \ell+1)}{C^\epsilon_E(\ell)} = \frac{C'_B(\ell, \ell+1)}{C^\epsilon_B(\ell)} = \frac{\ell}{2\pi^2} \sigma_\psi(\ell=1), \quad (42)$$

where we replaced ψ by σ_ψ as an order of magnitude estimate for a typical amplitude. Substituting numbers yields upper limits of 10% for the off-diagonal correlation relative to the diagonal ones at $\ell = 10^3$ which is smaller than the weak lensing shear at high redshifts, but comparable if not slightly larger than the lensing shear at low redshifts.

As the imprints of weak lensing on the intrinsic ellipticity pattern are basically identical to those in the case of lensing of the CMB polarisation, it is conceivable that the lensing deflection field can be estimated by measuring the amount of off-diagonal (meaning $\ell \neq \ell'$) spectra of the ellipticity modes as illustrated above, by applying the reconstruction technique worked out by Hu and Okamoto: With a model for intrinsic ellipticity spectra (which can be well predicted using a good prior on Ω_m , σ_8 , a and α) the statistics of the lensing deflection field can be inferred from broken homogeneity. In contrast to polarisation tensors, however, the ellipticity field is strongly shaped by shear and only in extreme cases such as a low-redshift galaxy sample at large multipoles the intrinsic alignment effects are dominant, where of course issues with the low surface density of lensing galaxies and the corresponding high Poisson-noise become important.

For illustration, Fig. 7 shows a realisation of the lensing potential with derived lensing deflections as gradients of the potential. The second derivatives have been used for generating a shear

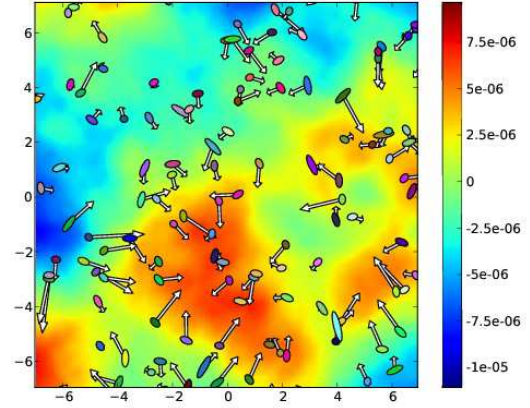


Figure 7. Realisation of a lensing potential on a $14^\circ \times 14^\circ$ -patch with 100 randomly sampled galaxies. The ellipticity is given by the lensing shear and the arrow indicates the apparent shift due to the weak lensing deflection. The realisation uses a lensing potential for the high-redshift galaxy sample with dominating shear. The displacement arrows are enhanced by a factor of 100 and the shears by a factor of 10, applied to a circular spot.

field that is depicted as a shape distortions of the otherwise circular spots. For visualisation, the deflections have been enlarged by a factor of 100 and the shear has been multiplied by 10.

4 SUMMARY

The subject of this work was an investigation of lensing effects and their observable signatures if the lensed galaxy sample shows intrinsic ellipticity correlations. Apart from weak lensing shear that operates on the shape of galaxies there will be a lensing deflection, which is unobservable in the case of uncorrelated ellipticities, but generates observable signatures if the lensing galaxies are intrinsically shape correlated. The lensing deflection manifests itself in the ellipticity spectra in three distinct ways: Firstly, there is a loss of amplitude in the spectra at high multipoles, secondly one observes a redistribution of amplitude between the E -mode and B -mode spectra, and thirdly there will be correlations between adjacent multipoles. In deriving these effects we made heavy use of analogies to the theory of lensing of the cosmic microwave background polarisation and identical mathematical properties of the ellipticity-polarisation tensors. In our investigation, we are comparing the forecasts for a high-redshift lensing survey such as EUCLID with a low-redshift galaxy sample in order to understand the scaling behaviour of all effects with distance.

(i) We derive ellipticity E -mode and B -mode spectra from a physical alignment model due to Crittenden et al. (2001). This model is quadratic in the tidal shear and applicable for describing shape correlations between isolated spiral galaxies. Due to the lack of an analytical description of how a galactic disk is oriented inside a dark matter halo we think of our spectra as upper limits as we assume perfect alignment of the symmetry axis of the galactic disk with the host halo's angular momentum direction. The two parameters that enter our ellipticity model, the alignment parameter a and the disk thickness α , are determined from numerical simulations and from observations of local galaxies.

(ii) The impact of lensing deflection on intrinsically shape-correlated galaxies is threefold: There is a smoothing of the intrinsic ellipticity spectra, a mixing in multipole and a conversion between E -modes and B -modes, and the generation of correlations between otherwise uncorrelated multipoles, as an expression of violated homogeneity of the lensed galaxy field.

(iii) By drawing analogies between galaxy ellipticities and the CMB-polarisation, namely that both are tensorial fields with spin-2, we can formulate transformation formulas for the ellipticity spectra, if individual galaxies have been coherently shifted to a new position by lensing. The transformation formula can be written concisely as a combined convolution and mode-mixing relation.

(iv) Lensing deflection operates on intrinsic ellipticity spectra by convolution. Correlation amplitudes are redistributed in multipoles which can be observed on small angular scales when intrinsic alignment spectra cease to be constant and drop in amplitude. Then, lensing causes the spectra to drop faster. Qualitatively, these effects are weak at high redshifts and dominated by far by the weak shear signal, but are sizable at low redshifts, where the weak lensing shear is small. In this case, weak lensing can actually weaken shape-correlations by random redistribution of intrinsically aligned galaxies.

(v) The losses in amplitude amount roughly to 5% in $C_E^\ell(\ell)$ and to 30% in $C_B^\ell(\ell)$ at $\ell = 3000$ in the case of the high redshift sample and at $\ell = 1000$ in the case of the low redshift sample. Compared to the convolution of the spectra the conversion between E - and B -modes is a minor effect.

(vi) We have derived an upper limit on the correlation between different multipoles due to broken homogeneity by using the fact that the correlations with between adjacent multipoles should be strongest. These correlations can be estimated to be at most $\sim 10\%$ of the spectra at the largest multipoles, both for E - and B -modes, and are proportional to ℓ .

(vii) Although we could take advantage of formal analogies between the CMB-polarisation and ellipticity fields, concerning symmetry properties, the description with spectra and the incorporation of the lensing effect we would like to emphasise that that in contrast to the CMB, lensing does not introduce a bispectrum into the ellipticity correlations. The CMB-lensing bispectrum is sourced by the integrated Sachs-Wolfe effect in the same potential that causes the lensing-deflection (Hu 2000), and there is no analogous mechanism in the case of galaxy ellipticities.

We conclude that for deep-reaching lensing surveys intrinsic alignments are subdominant and that the shaping of their correlations by weak lensing deflection (and by peculiar motion, which is of a similar order of magnitude, see Giali-Saravani & Schäfer 2012) is small compared to gravitational shear. At low redshifts, however, the situation is inverted: Intrinsic alignments dominate and the most important lensing effect is deflection. In contrast to the CMB-polarisation, it is doubtful if a violation of homogeneity of the ellipticity field introduced by lensing can be observed.

ACKNOWLEDGEMENTS

Our work was supported by the German Research Foundation (DFG) within the framework of the excellence initiative through the Heidelberg Graduate School of Fundamental Physics. In particular, AGS acknowledges funding from the FRONTIER-programme, from the International Max Planck Research School for Cosmic Physics and from the Heidelberg Graduate School for Fundamental Physics. We would like to thank Philipp M. Merkel for his insight

into CMB-lensing reconstructions and numerical advice, which he shared with us, and Vanessa M. Böhm for valuable comments.

REFERENCES

- Abramowitz M., Stegun I. A., 1972, Handbook of Mathematical Functions. Handbook of Mathematical Functions, New York: Dover, 1972
- Amara A., Réfrégier A., 2007, MNRAS, 381, 1018
- Andrae R., Jahnke K., 2011, MNRAS, p. 1665
- Arfken G. B., Weber H. J., 2005, Materials and Manufacturing Processes
- Bailin J., Kawata D., Gibson B. K., Steinmetz M., Navarro J. F., Brook C. B., Gill S. P. D., Ibata R. A., Knebe A., Lewis G. F., Okamoto T., 2005, ApJL, 627, L17
- Bardeen J. M., Bond J. R., Kaiser N., Szalay A. S., 1986, ApJ, 304, 15
- Bartelmann M., 2010, Classical and Quantum Gravity, 27, 233001
- Bartelmann M., Schneider P., 2001, Physics Reports, 340, 291
- Bernardeau F., Bonvin C., Vernizzi F., 2010, Phys. Rev. D, 81, 083002
- Bernstein G. M., 2009, ApJ, 695, 652
- Blazek J., McQuinn M., Seljak U., 2011, JCAP, 5, 10
- Bridle S., King L., 2007, New Journal of Physics, 9, 444
- Bullock J. S., Dekel A., Kolatt T. S., Kravtsov A. V., Klypin A. A., Porciani C., Primack J. R., 2001, ApJ, 555, 240
- Capranico F., Merkel P. M., Schäfer B. M., 2012, ArXiv e-prints 1207.5939
- Carbone C., Baccigalupi C., Bartelmann M., Matarrese S., Springel V., 2009, MNRAS, 396, 668
- Catelan P., 1995, MNRAS, 276, 115
- Catelan P., Kamionkowski M., Blandford R. D., 2001, MNRAS, 320, L7
- Catelan P., Porciani C., 2001, MNRAS, 323, 713
- Catelan P., Theuns T., 1996a, MNRAS, 282, 436
- Catelan P., Theuns T., 1996b, MNRAS, 282, 455
- Challinor A., Lewis A., 2005, Phys. Rev. D, 71, 103010
- Codis S., Pichon C., Devriendt J., Slyz A., Pogosyan D., Dubois Y., Sousbie T., 2012, ArXiv e-prints 1201.5794
- Cooray A., Hu W., 2002, ApJ, 574, 19
- Crittenden R. G., Natarajan P., Pen U.-L., Theuns T., 2001, ApJ, 559, 552
- Crittenden R. G., Natarajan P., Pen U.-L., Theuns T., 2002, ApJ, 568, 20
- Croft R. A. C., Metzler C. A., 2000, ApJ, 545, 561
- Doroshkevich A. G., 1970, Astrofizika, 6, 581
- Fu L., Kilbinger M., 2010, MNRAS, 401, 1264
- Giali-Saravani A., Schäfer B. M., 2012, ArXiv e-prints 1202.1196
- Godłowski W., 2012, ApJ, 747, 7
- Hahn O., Carollo C. M., Porciani C., Dekel A., 2007, MNRAS, 381, 41
- Hamana T., Bartelmann M., Yoshida N., Pfrommer C., 2005, MNRAS, 356, 829
- Heavens A., Refregier A., Heymans C., 2000, MNRAS, 319, 649
- Heymans C., Brown M., Heavens A., Meisenheimer K., Taylor A., Wolf C., 2004, MNRAS, 347, 895
- Heymans C., Heavens A., 2003, MNRAS, 339, 711
- Hirata C. M., Mandelbaum R., Ishak M., Seljak U., Nichol R., Pimbblet K. A., Ross N. P., Wake D., 2007, MNRAS, 381, 1197

- Hirata C. M., Mandelbaum R., Seljak U., Guzik J., Padmanabhan N., Blake C., Brinkmann J., Budávári T., Connolly A., Csabai I., Scranton R., Szalay A. S., 2004, *MNRAS*, 353, 529
- Hirata C. M., Seljak U., 2004, *Phys. Rev. D*, 70, 063526
- Hoekstra H., Jain B., 2008, *Annual Review of Nuclear and Particle Science*, 58, 99
- Hoyle F., 1949, *MNRAS*, 109, 365
- Hu W., 2000, *Phys. Rev. D*, 62, 043007
- Hu W., White M., 2001, *ApJ*, 554, 67
- Joachimi B., Bridle S. L., 2010, *A&A*, 523, A1
- Joachimi B., Mandelbaum R., Abdalla F. B., Bridle S. L., 2011, *A&A*, 527, A26
- Joachimi B., Schneider P., 2008, *ArXiv e-prints* 0804.2292, 804
- Joachimi B., Schneider P., 2010a, *ArXiv e-prints* 1009.2024
- Joachimi B., Schneider P., 2010b, *A&A*, 517, A4
- Kaiser N., 1992, *ApJ*, 388, 272
- King L., Schneider P., 2002, *A&A*, 396, 411
- King L. J., 2005, *A&A*, 441, 47
- King L. J., Schneider P., 2003, *A&A*, 398, 23
- Kirk D., Bridle S., Schneider M., 2010, *MNRAS*, 408, 1502
- Kirk D., Laszlo I., Bridle S., Bean R., 2011, *ArXiv e-prints* 1109.4536
- Kirk D., Rassat A., Host O., Bridle S., 2012, *MNRAS*, 424, 1647
- Kitching T. D., Taylor A. N., 2011, *MNRAS*, 410, 1677
- Krause E., Hirata C. M., 2009, *ArXiv e-prints* 0910.3786
- Lee J., 2013, *ArXiv e-prints* 1301.0348
- Lee J., Pen U.-L., 2001, *ApJ*, 555, 106
- Lee J., Pen U.-L., 2002, *ApJL*, 567, L111
- Lee J., Pen U.-L., 2007, *ApJL*, 670, L1
- Lee J., Pen U.-L., 2008, *The Astrophysical Journal*, 681, 798
- Lee J., Springel V., Pen U.-L., Lemson G., 2007, *ArXiv* 0709.1106, 709
- Lewis A., Challinor A., 2006, *Physics Reports*, 429, 1
- Libeskind N. I., Hoffman Y., Steinmetz M., Gottloeber S., Knebe A., Hess S., 2012, *ArXiv e-prints* 1212.1454
- Limber D. N., 1954, *ApJ*, 119, 655
- Linder E. V., Jenkins A., 2003, *MNRAS*, 346, 573
- Mackey J., White M., Kamionkowski M., 2002, *MNRAS*, 332, 788
- Mandelbaum R., Blake C., Bridle S., Abdalla F. B., Brough S., Colless M., Couch W., Croom S., et al., 2011, *MNRAS*, 410, 844
- Mandelbaum R., Hirata C. M., Ishak M., Seljak U., Brinkmann J., 2006, *MNRAS*, 367, 611
- Merkel P. M., Schäfer B. M., 2011, *MNRAS*, 411, 1067
- Natarajan P., Crittenden R. G., Pen U.-L., Theuns T., 2001, *Publications of the Astronomical Society of Australia*, 18, 198
- Okumura T., Jing Y. P., 2009, *ApJL*, 694, L83
- Peebles P. J. E., 1969, *ApJ*, 155, 393
- Pen U.-L., Lee J., Seljak U., 2000, *ApJL*, 543, L107
- Porciani C., Dekel A., Hoffman Y., 2002a, *MNRAS*, 332, 325
- Porciani C., Dekel A., Hoffman Y., 2002b, *MNRAS*, 332, 339
- Schäfer B. M., 2009, *International Journal of Modern Physics D*, 18, 173
- Schäfer B. M., Merkel P. M., 2012, *MNRAS*, 421, 2751
- Schneider M. D., Bridle S., 2010, *MNRAS*, 402, 2127
- Schneider P., Kilbinger M., 2007, *A&A*, 462, 841
- Schneider P., van Waerbeke L., Mellier Y., 2002, *A&A*, 389, 729
- Sciamia D. W., 1955, *MNRAS*, 115, 2
- Seljak U., 1996, *ApJ*, 463, 1
- Semboloni E., Heymans C., van Waerbeke L., Schneider P., 2008, *ArXiv* 0802.3978, 802
- Shapiro C., Cooray A., 2006, *Journal of Cosmology and Astro-Particle Physics*, 3, 7
- Smith R. E., Peacock J. A., Jenkins A., White S. D. M., Frenk C. S., Pearce F. R., Thomas P. A., Efstathiou G., Couchman H. M. P., 2003, *MNRAS*, 341, 1311
- Stewart K. R., Brooks A. M., Bullock J. S., Maller A. H., Diemand J., Wadsley J., Moustakas L. A., 2013, *ArXiv e-prints*
- Sugiyama N., 1995, *ApJS*, 100, 281
- Turner M. S., White M., 1997, *Phys. Rev. D*, 56, 4439
- Wang L., Steinhardt P. J., 1998, *ApJ*, 508, 483
- Weinberg D. H., Mortonson M. J., Eisenstein D. J., Hirata C., Riess A. G., Rozo E., 2012, *ArXiv e-prints* 1201.2434
- White S. D. M., 1984, *ApJ*, 286, 38
- Zhang P., 2010, *ApJ*, 720, 1090

This paper has been typeset from a \LaTeX file prepared by the author.